Science Advances
AAAS

Supplementary Materials for

The reduced net carbon uptake over Northern Hemisphere land causes the close-to-normal CO_2 growth rate in 2021 La Niña

Junjie Liu *et al.*

Corresponding author: Junjie Liu, junjie.liu@jpl.nasa.gov

Sci. Adv. **10**, eadl2201 (2024)
DOI: 10.1126/sciadv.adl2201

This PDF file includes:

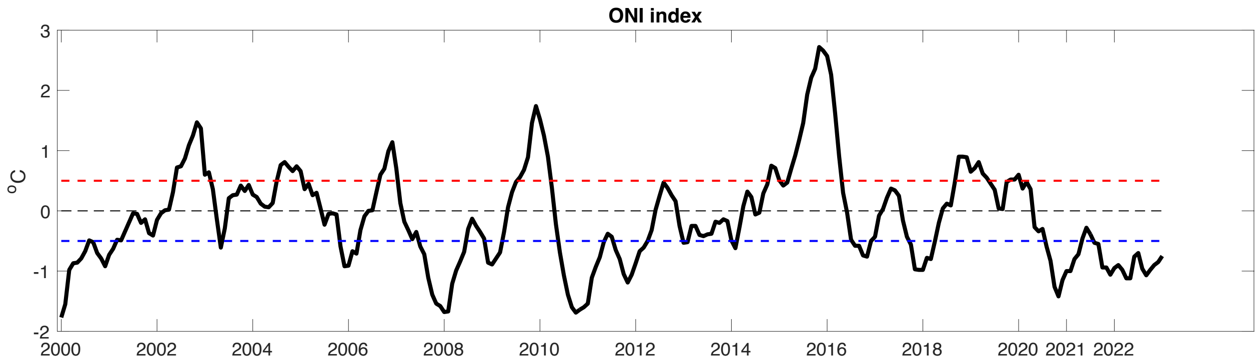

Fig. S1. Monthly Oceanic Niño Index (ONI) between Jan 2000- Jan 2023 (unit: °C). It is defined as monthly running mean sea surface temperature (SST) anomalies in the Niño 3.4 region (5ºN-5ºS, 120º-170ºW). When ONI index is lower than -0.5°C, it is defined as La Niña, and it is El Niño when ONI index is higher than 0.5°C. 2021 is in the middle of the longest La Niña in this century.

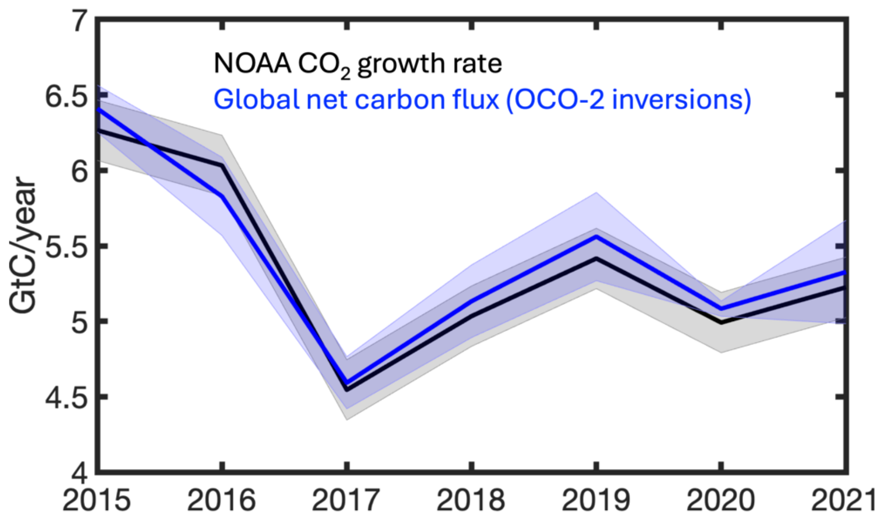

Figure S2 Comparison between NOAA global CO_2 growth rate and the annual net carbon flux based on the ensemble OCO-2 inversions. The annual net carbon fluxes were calculated as the sum of fossil fuel emissions and natural carbon fluxes over land and ocean, which represent the total changes of atmospheric CO_2 estimated by inversion models. The NOAA global CO_2 growth rate was converted to gigaton carbon per year using the conversion factor of 2.124GtC/ppm (42). We assumed 0.2 GtC/year uncertainty for the observed NOAA annual CO_2 growth following (17), while the ensemble model spread was used as the uncertainty for the inversion results.

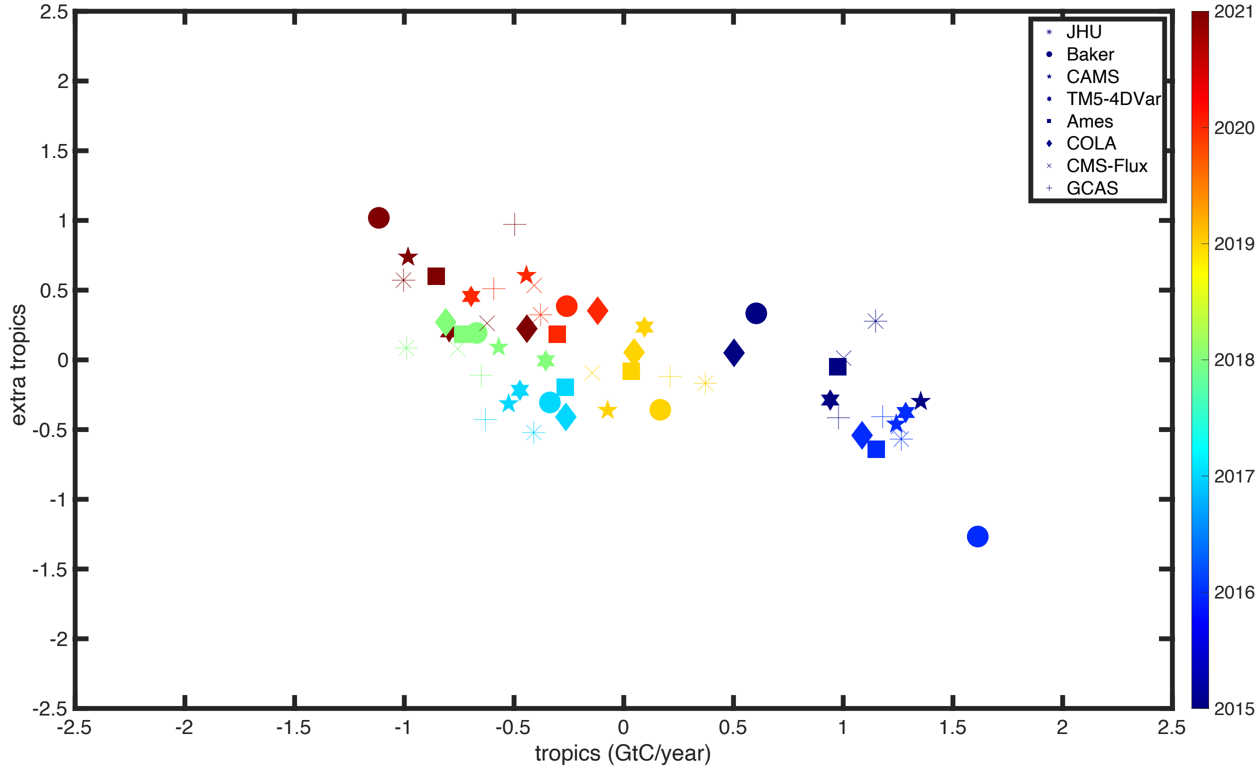

Figure S3 The annual net biosphere exchange (NBE) anomalies over the tropics and extra-tropics estimated by the eight inversion models, which are JHU, Baker, CAMS, TM5-4DVar, AMES, COLA, CMS-Flux, and GCAS. The color represents years. Unit: GtC/year.

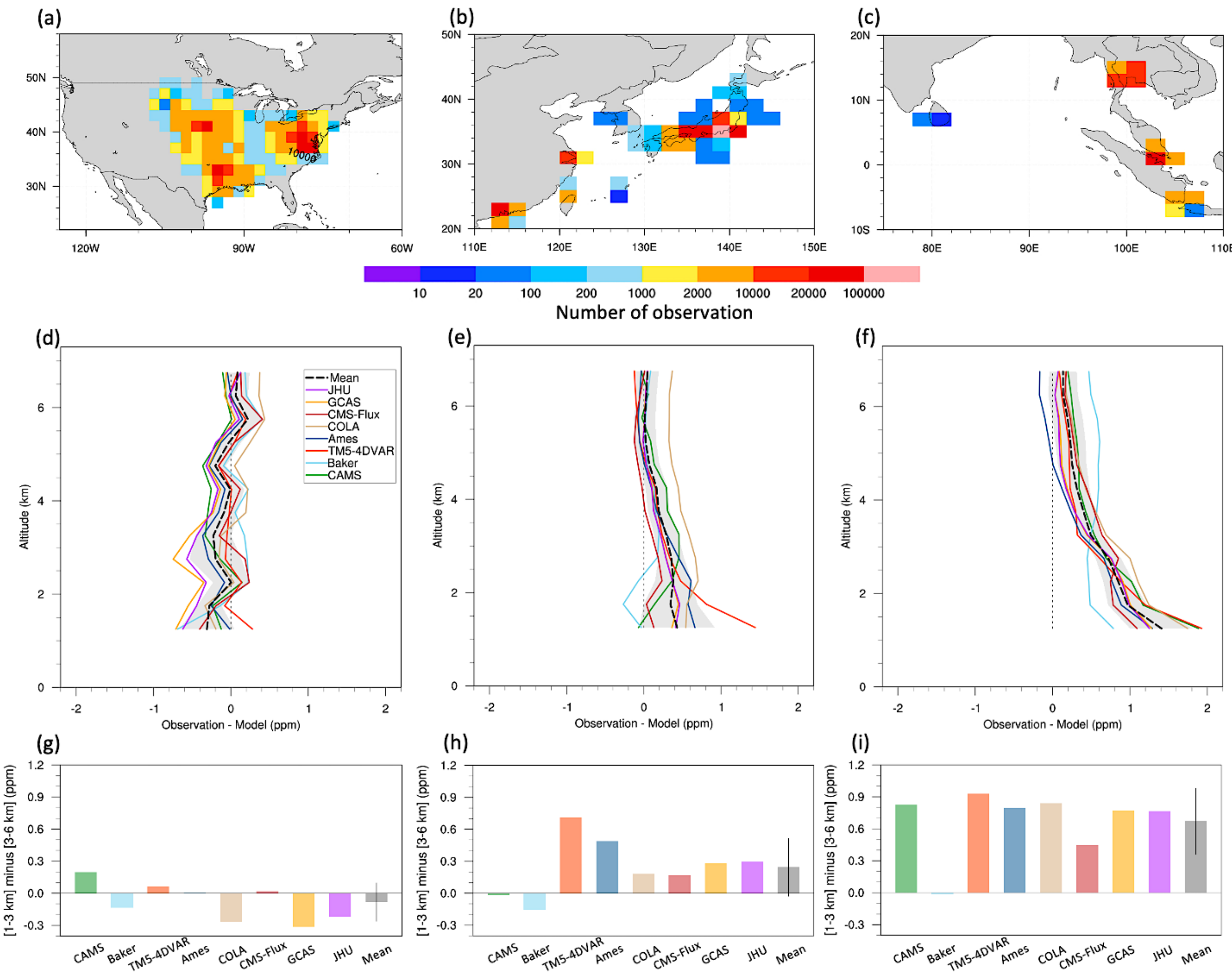

Figure S4 Spatial distributions of the number of aircraft atmospheric CO_2 observations from 1 km to 7 km over mid-latitude North America (a), East Asia (b), and Southeast Asia (c) for the period 2015-2019. The aircraft observations are from the Atmospheric Carbon and Transport (ACT) – America and Comprehensive Observation Network for TRace gases by AIrLiner (CONTRAIL) projects (46). (d-f) Mean atmospheric CO_2 differences with a 0.5 km interval between observations and OCO-2 MIP models over each region for the same period. Black line and shaded area denote ensemble mean and one inter-model standard deviation range. (g-i) Vertical gradients of mean observation-model differences of atmospheric CO_2 for altitude ranges of 1-3 km and 3-6 km above ground.

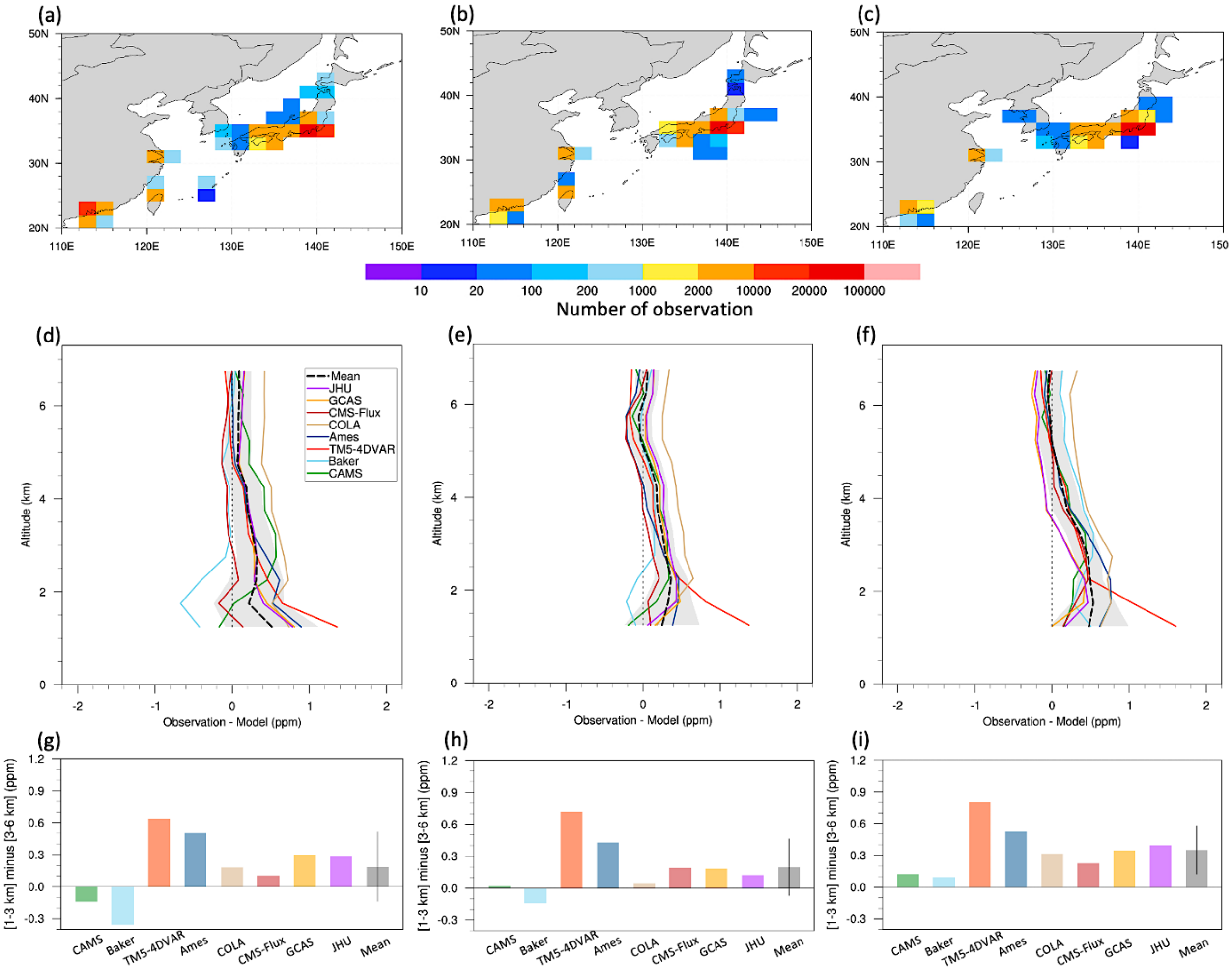

Figure S5 Same as Figure S4 but for aircraft atmospheric CO_2 observations over East Asia for 2015 (a, d, and g), 2016 (b, e, and h), and 2017 (c, f, and i).

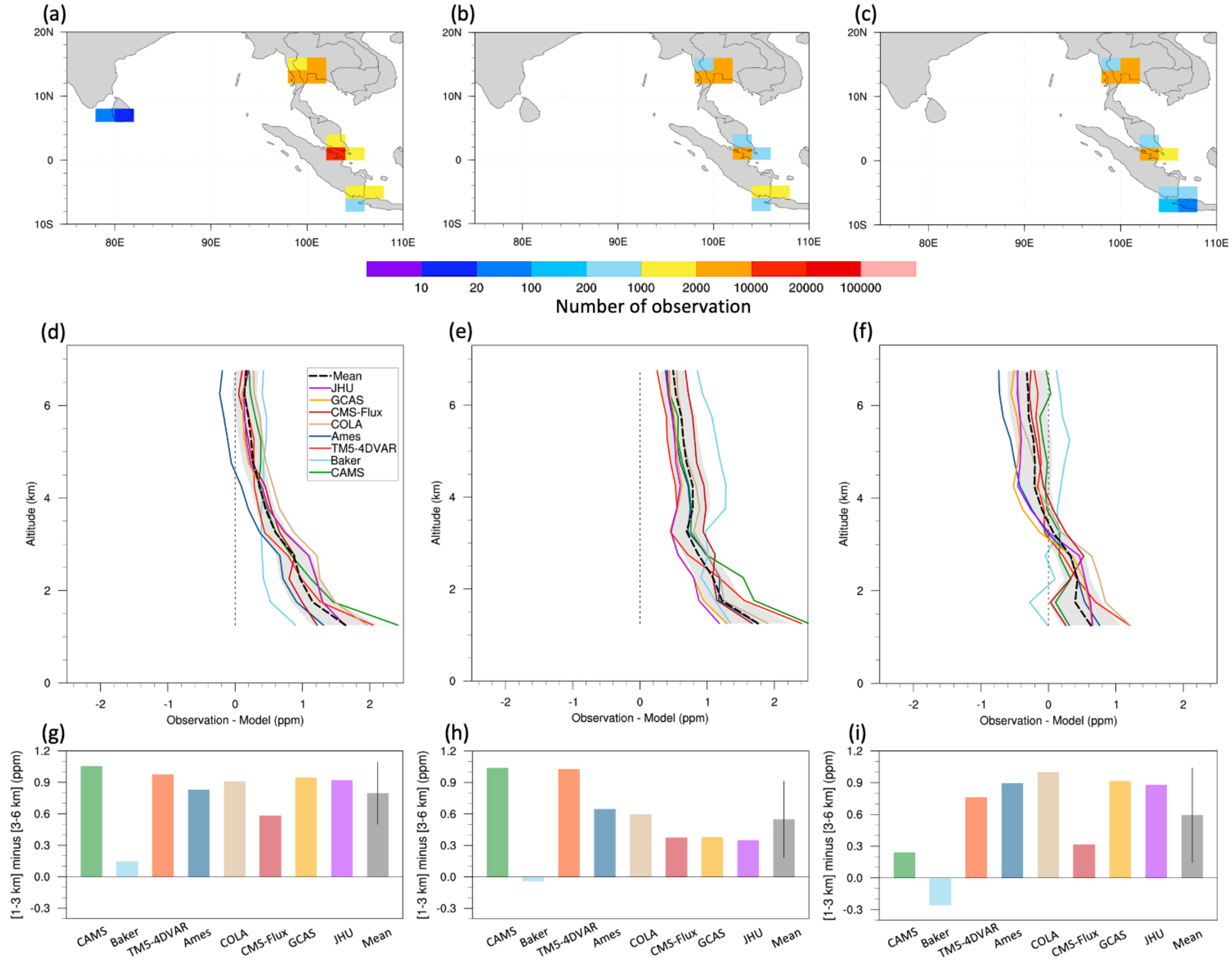

Figure S6 Same as Figure S4 but for aircraft atmospheric CO_2 observations over Southeast Asia for 2015 (a, d, g), 2016 (b, e, and h), and 2017 (c, f, and i).

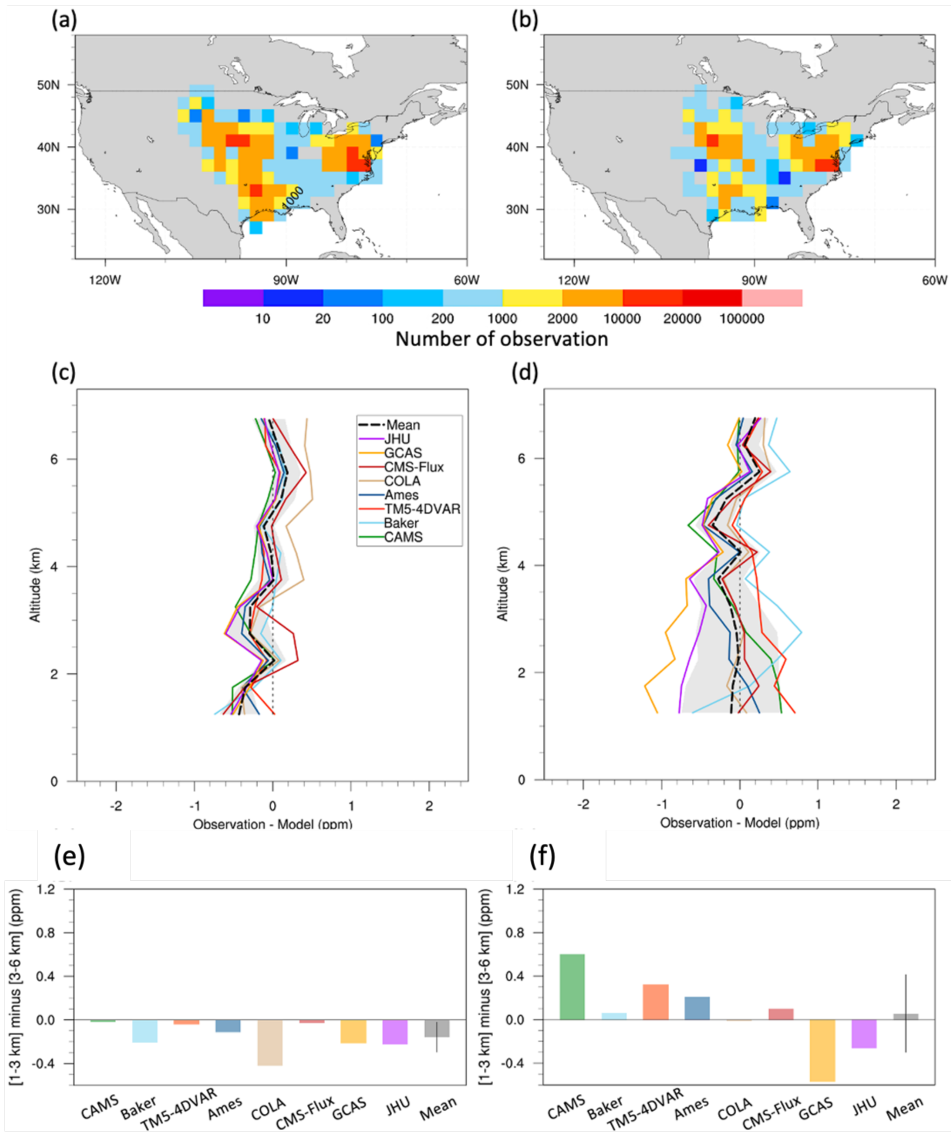

Figure S7 Same as Figure S4 but for aircraft atmospheric CO_2 observations over mid-latitude North America for the periods 2016-2017 (a, c, and e) and 2018-2019 (b, d, and f).

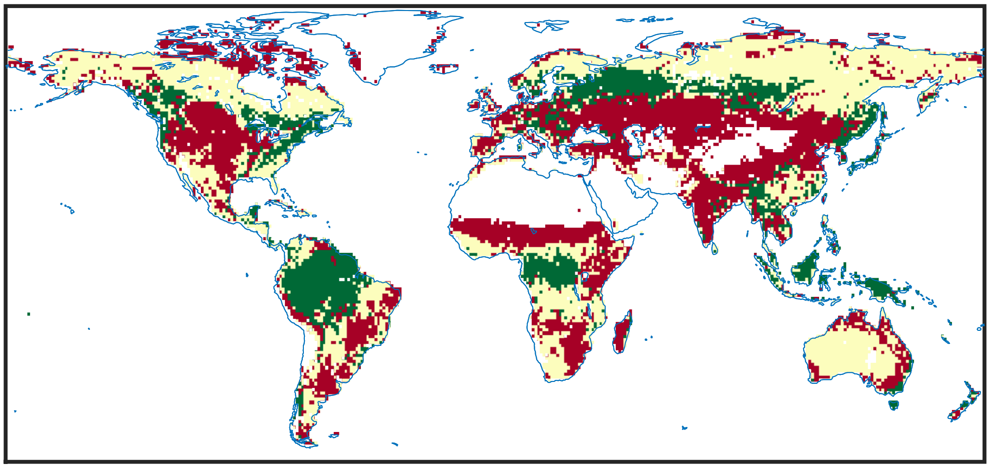

Fig. S8 Land cover classification based on MODIS International Geosphere – Biosphere Program (IGBP) 2020 data. Green: forest; yellow: semi-arid region; and red: grassland and cropland. Forest type includes evergreen needleleaf forest, evergreen broadleaf forest, deciduous needleleaf forest, deciduous broadleaf forest and mixed forest. Semiarid region includes grid points dominated by closed shrublands, open shrublands, woody savannas, and savannas.

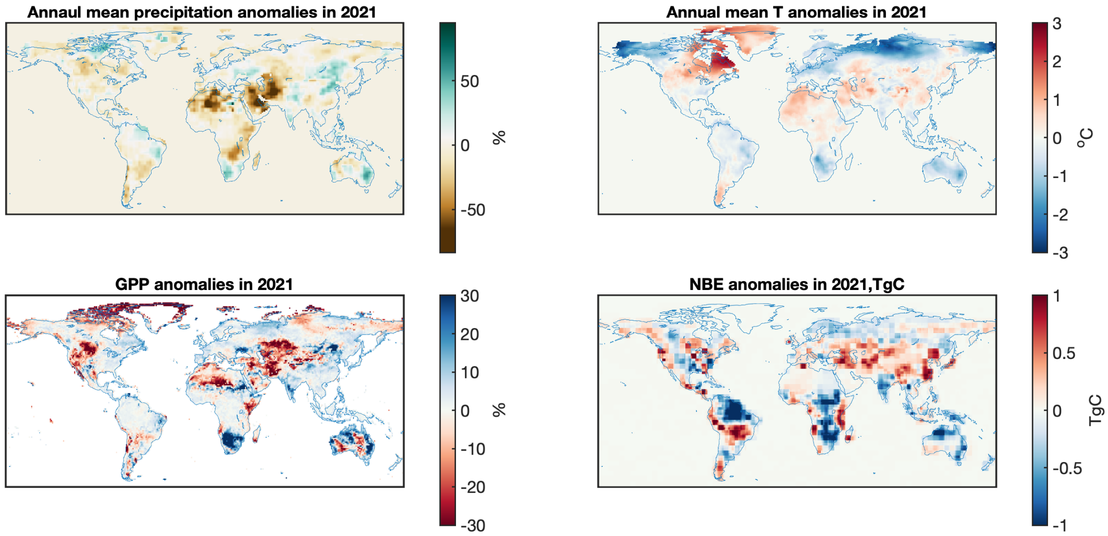

Fig. S9 Spatial distributions of annual climate and carbon flux anomalies. Top left panel: Percentage of annual precipitation anomalies (unit: %); top right panel : annual temperature anomalies (unit: °C); bottom left panel: percentage of GPP anomalies (unit: %); bottom right panel: annual anomalies of net biosphere exchange (unit: tera grams of carbon; TgC).

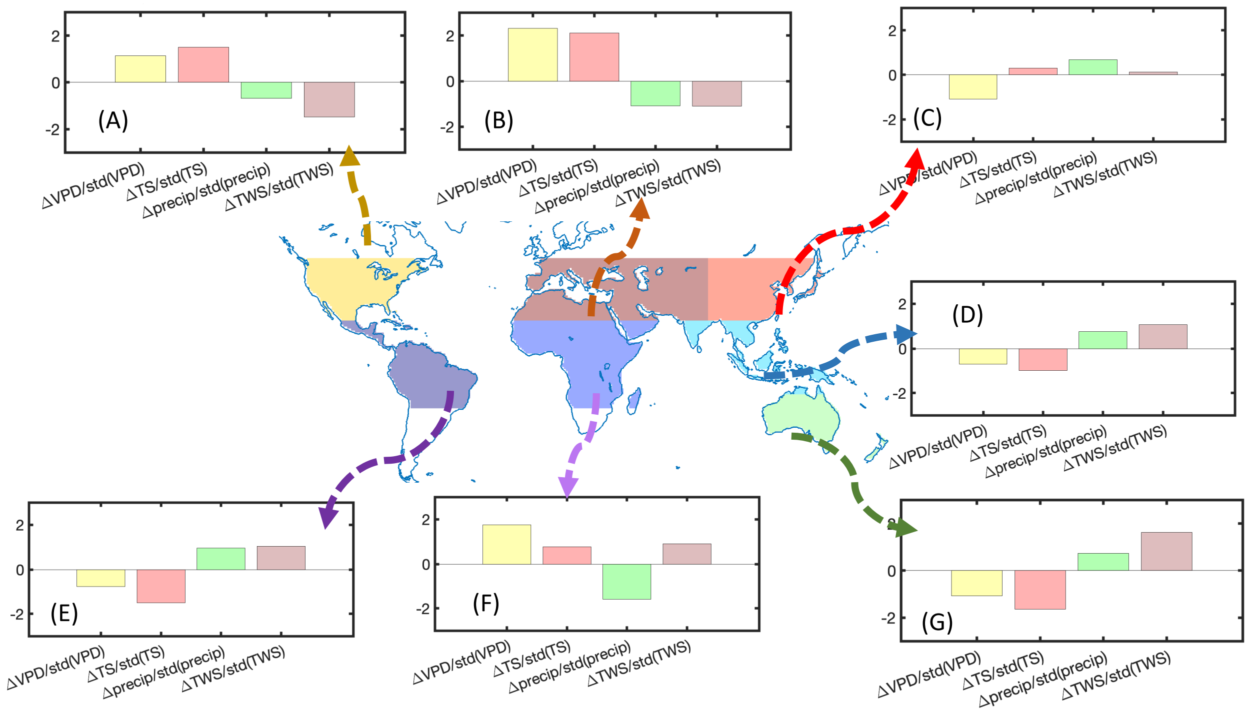

Figure S10 Regional normalized climate anomalies. Normalized annual anomalies of vapor pressure deficit (VPD) (yellow), surface temperature (Ts) (red), precipitation (green), and total water storage (TWS)anomalies (brown) over mid latitudes of North America (NA) (A), Eurasia (B), East Asia (C), tropical Asia (D), rest of Australia (G), tropical Africa (F), and tropical South America (E) (clockwise). The normalized anomalies are defined as the ratio between annual anomalies in 2021 and standard deviation of annual anomalies over 2015-2021. For TWS, the standard deviation was calculated over 2015-2016 and 2019-2021 due to missing data in 2017 and 2018.

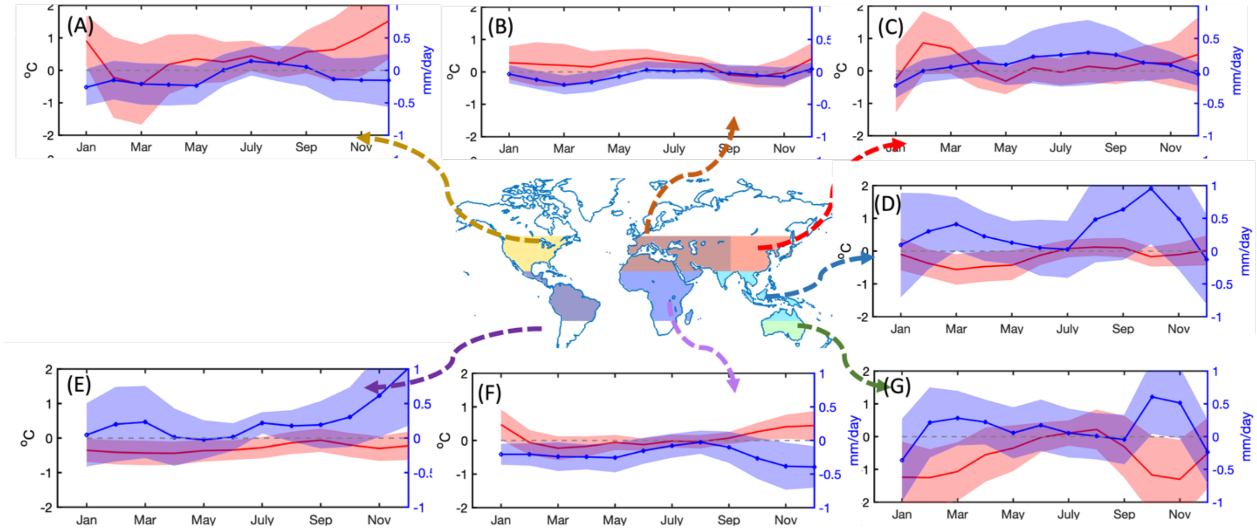

Figure S11 Regional monthly climate anomalies in 2021. Monthly anomalies of temperature (red, unit: °C) and precipitation (blue, unit: mm/day) over mid latitudes of North America (NA) (A), Eurasia (B), East Asia (C), tropical Asia (D), the rest of Australia (G), tropical Africa (F), and tropical South America (E) (clockwise). The shaded area represents monthly variations of regional mean temperature or precipitation between 2015-2021.

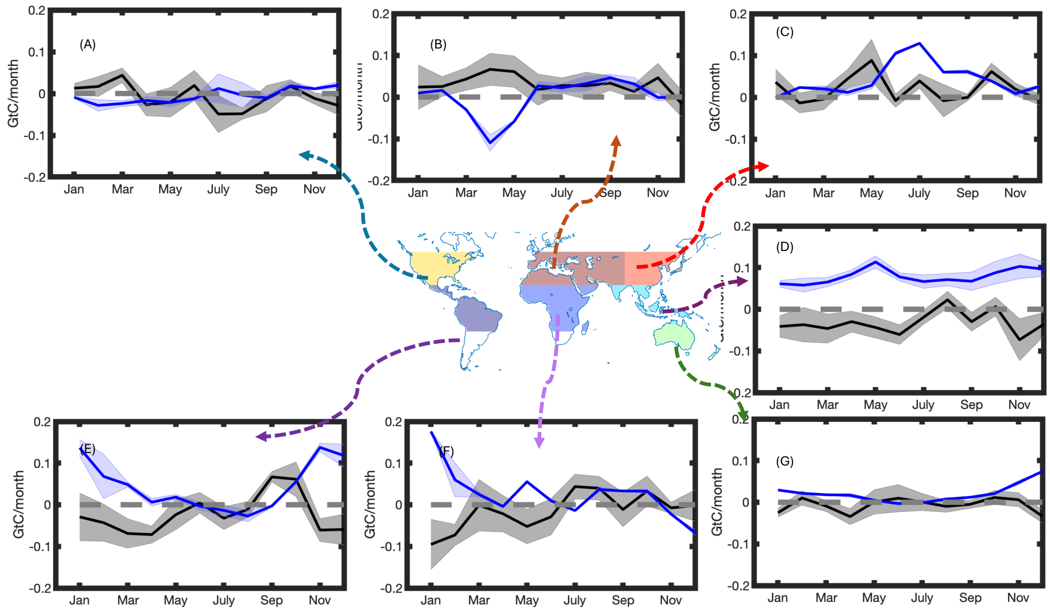

Figure S12 Regional monthly carbon flux anomalies in 2021. Monthly anomalies of gross primary production (GPP) (blue, unit: GtC/month) and net biosphere exchange (NBE) (black, unit: GtC/month) over mid latitudes of North America (NA) (A), Eurasia (B), East Asia (C), tropical Asia (D), the rest of Australia (G), tropical Africa (F), and tropical South America (E) (clockwise).

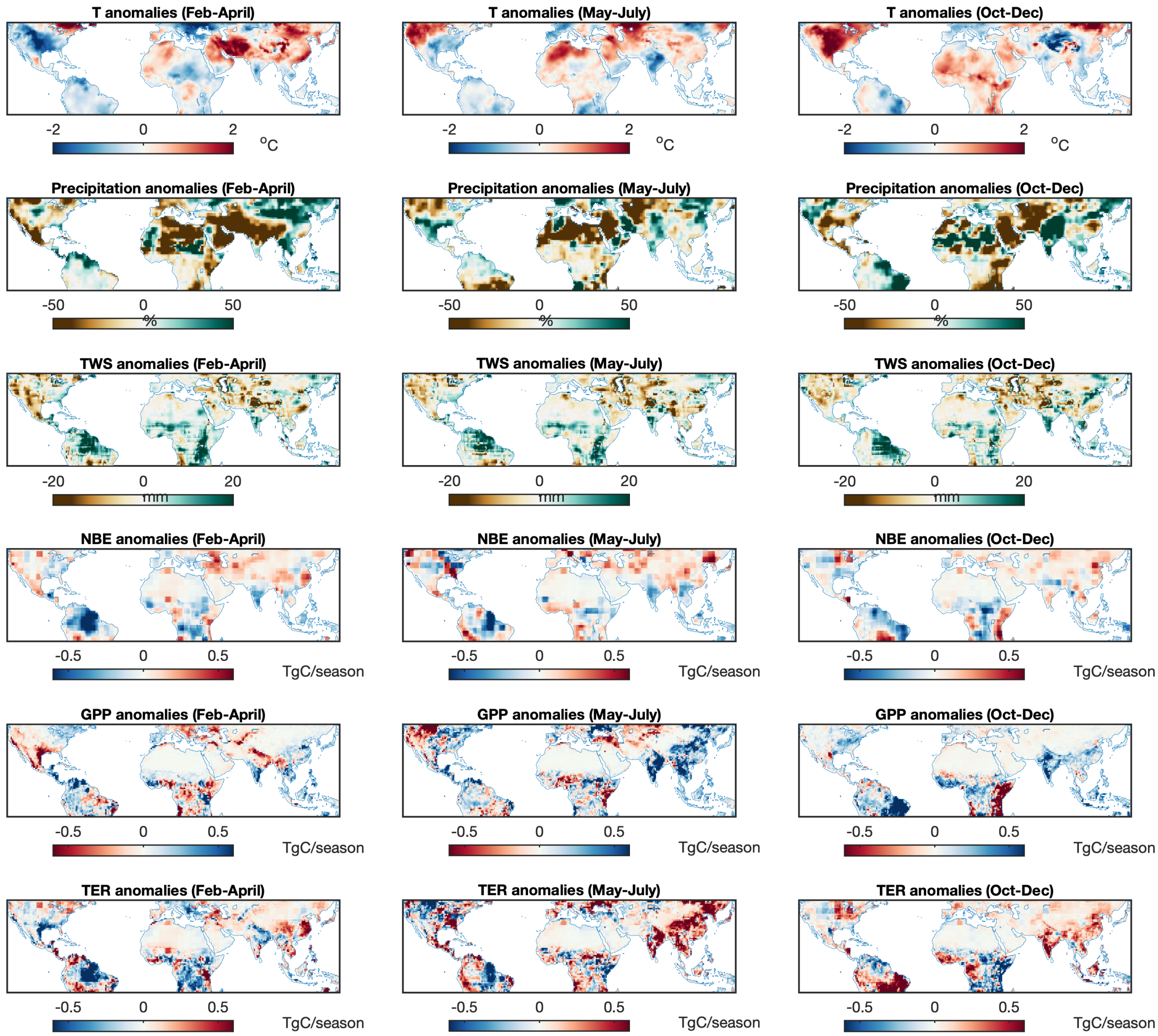

Figure S13 Temperature (top row), precipitation (second row), total water storage deficit (third row), net biosphere exchange (NBE) (fourth row), gross primary production (GPP) (fifth row), and total ecosystem respiration (TER) (sixth row) anomalies over Feb-April (left column), May-July (middle column), and Oct-Dec (right column) in 2021.

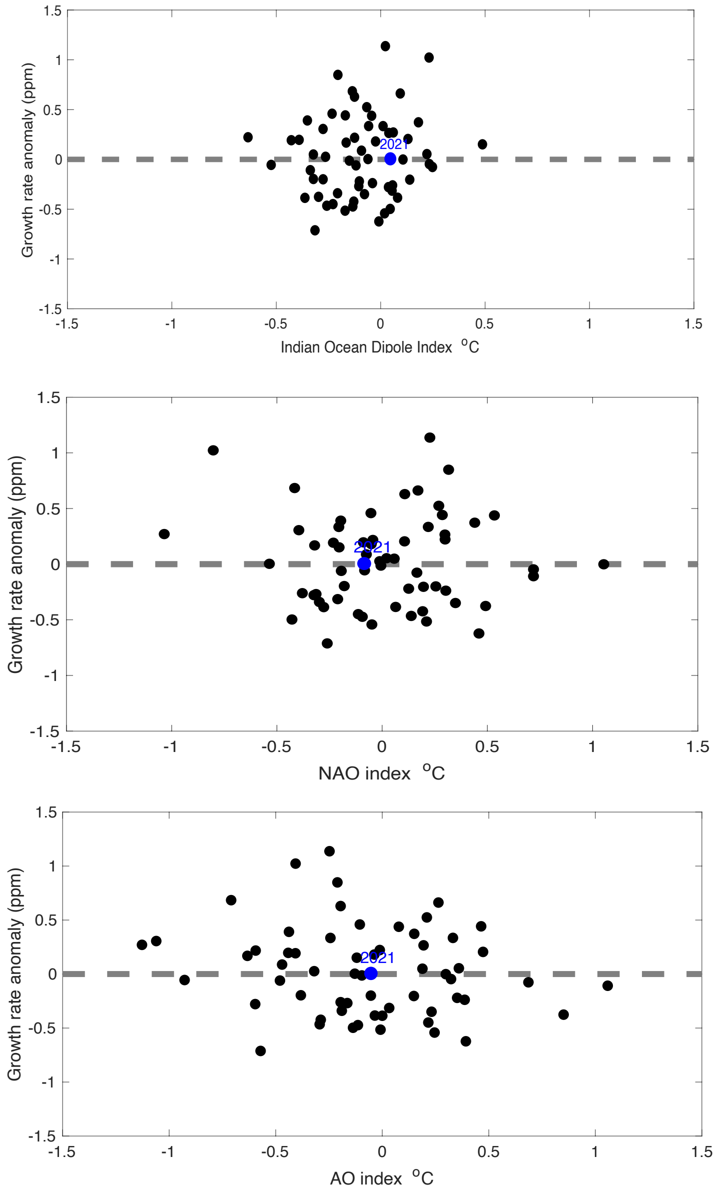

Figure S14 Top panel: annual mean Indian Ocean Dipole (IOD) Index vs. CO_2 growth rate anomaly between 1959-2021 without 1991 and 1992, when Pinatubo volcano eruption had a dominant impact. The Indian Ocean Dipole index data was downloaded from https://psl.noaa.gov/gcos_wgsp/Timeseries/DMI/. Middle panel: annual mean North Atlantic Oscillation (NAO) Index vs. CO_2 growth rate anomaly between 1959-2021 without 1991 and 1992. The NAO index data was downloaded from https://www.cpc.ncep.noaa.gov/products/precip/CWlink/pna/nao.shtml. Bottom panel: annual mean Arctic Oscillation (AO) Index vs. CO_2 growth rate anomaly between 1959-2021 without 1991 and 1992. The AO index data was downloaded from https://www.cpc.ncep.noaa.gov/products/precip/CWlink/daily_ao_index/ao.shtml.

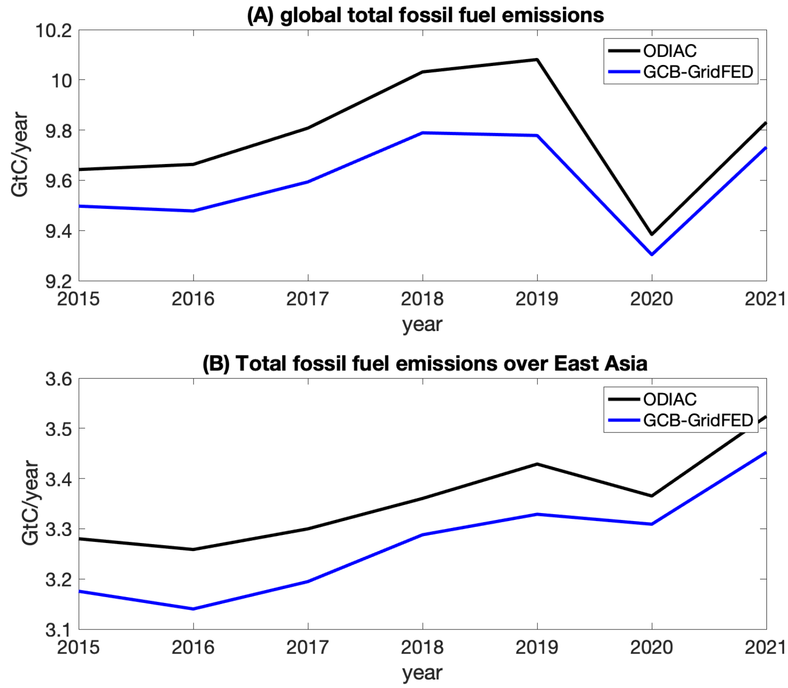

Figure S15 The Open-source Data Inventory for Atmospheric CO2 (ODIAC) fossil fuel emissions used in this study and the Gridded Fossil fuel Emission Dataset (GridFED) from global carbon budget 2022 (GCB-GridFED) have the similar changes during 2015-2021, though the mean difference is about 0.1 GtC/year. (A): global fossil fuel emission estimates from ODIAC (black) and GCB-GridFED (blue); (B): total fossil fuel emissions over East Asia. Unit: GtC/year.

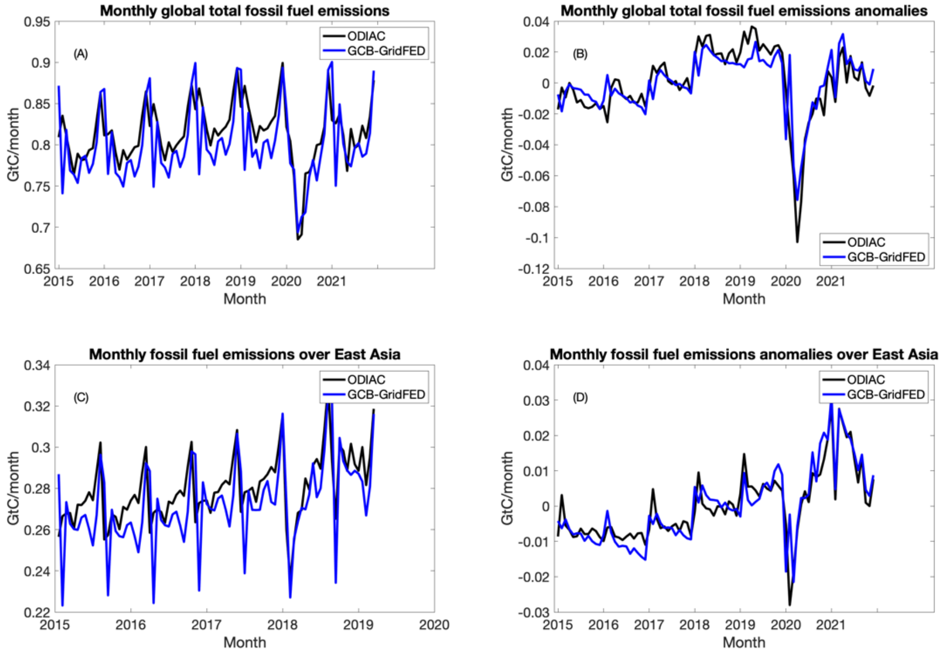

Figure S16 The Open-source Data Inventory for Atmospheric CO2 (ODIAC) fossil fuel emissions used in this study and the Gridded Fossil fuel Emission Dataset (GridFED) from global carbon budget 2022 (GCB-GridFED) have the similar monthly anomalies in both global scale and over East Asia, though these two fossil fuel emissions have different seasonal cycle. (A) Monthly global fossil fuel emission estimates from ODIAC (black) and GCB-GridFED (blue) and (B) their anomalies. (C) Monthly fossil fuel emissions over East Asia and (D) their anomalies. Unit: GtC/month.

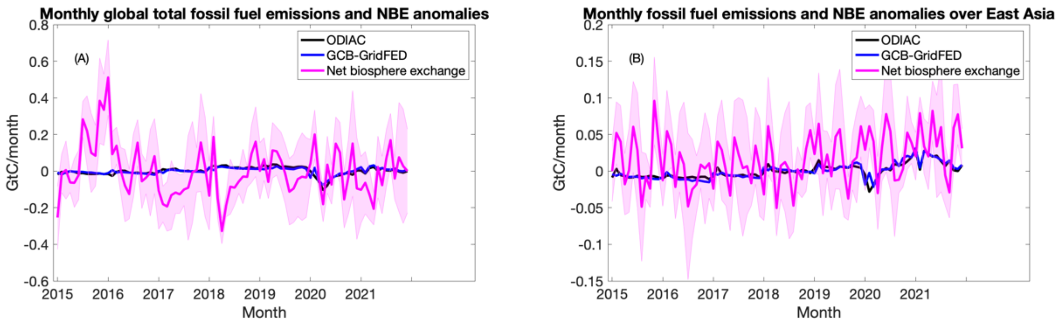

Figure S17 The contrast between monthly net biosphere exchange (NBE) anomalies and monthly fossil fuel emission anomalies. (A) Monthly fossil fuel emission anomalies from the Open-source Data Inventory for Atmospheric CO2 (ODIAC) (black) and the Gridded Fossil fuel Emission Dataset (GridFED) from global carbon budget 2022 (GCB-GridFED) (blue), and NBE anomalies (magenta) over the globe and (B) over East Asia. Unit: GtC/month.

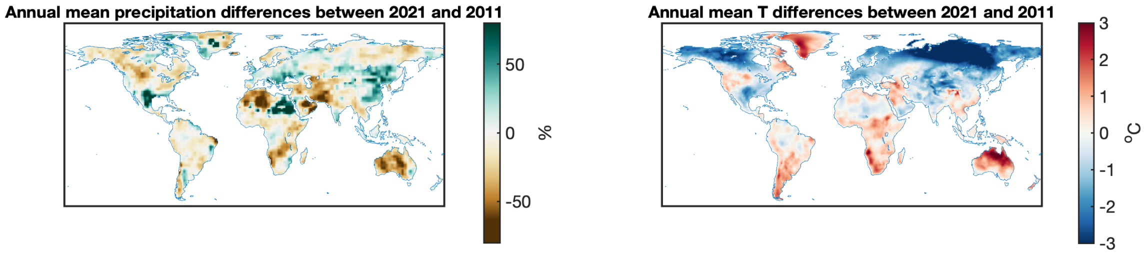

Figure S18 Left panel: annual mean relative precipitation differences between 2021 and 2011 (unit: %). The precipitation differences are normalized by the annual mean precipitation between 2015-2021. Right panel: annual mean temperature differences between 2021 and 2011 (unit: °C).

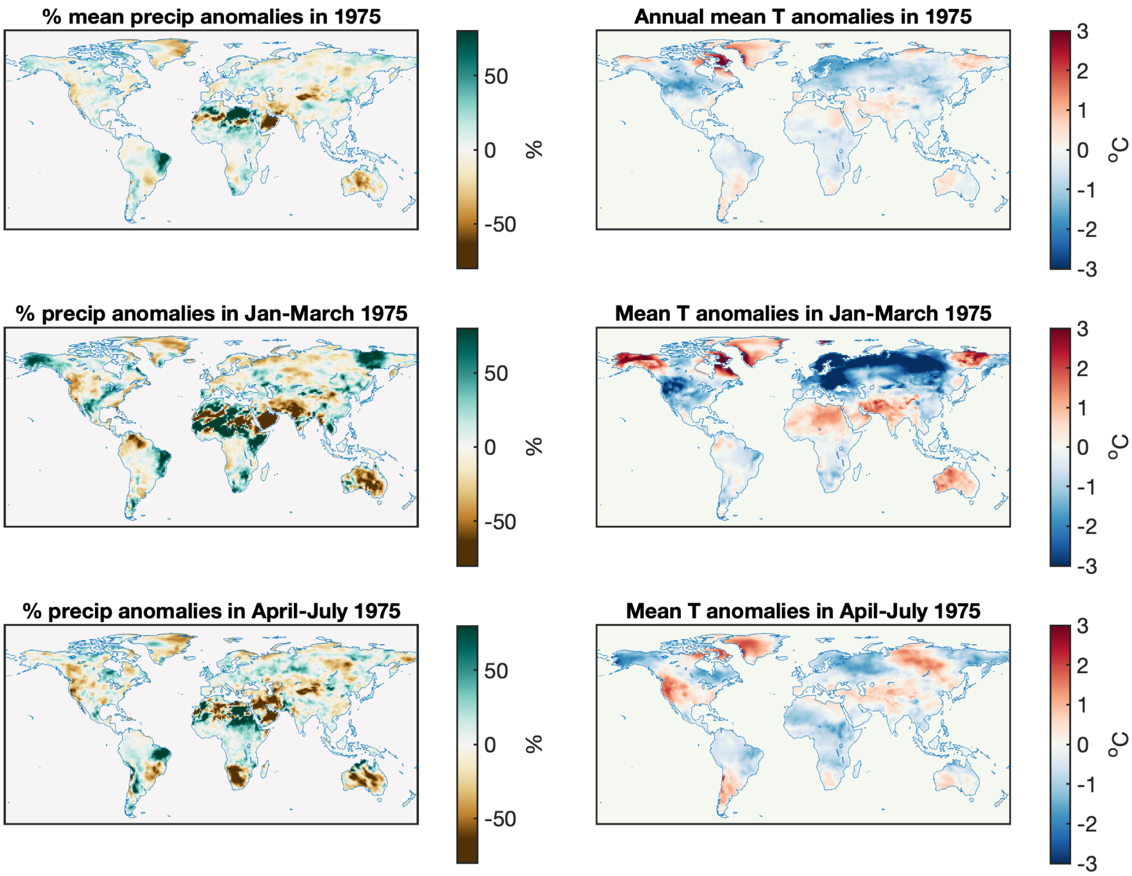

Figure S19 Precipitation and temperature anomalies in 1975. The anomalies were calculated with respect to the mean between 1972 and 1978. Top panels: annual precipitation and temperature anomalies (unit: °C); Middle panel: precipitation and temperature anomalies between Jan-March 1975; Bottom panel: precipitation and temperature anomalies between April-July 1975.

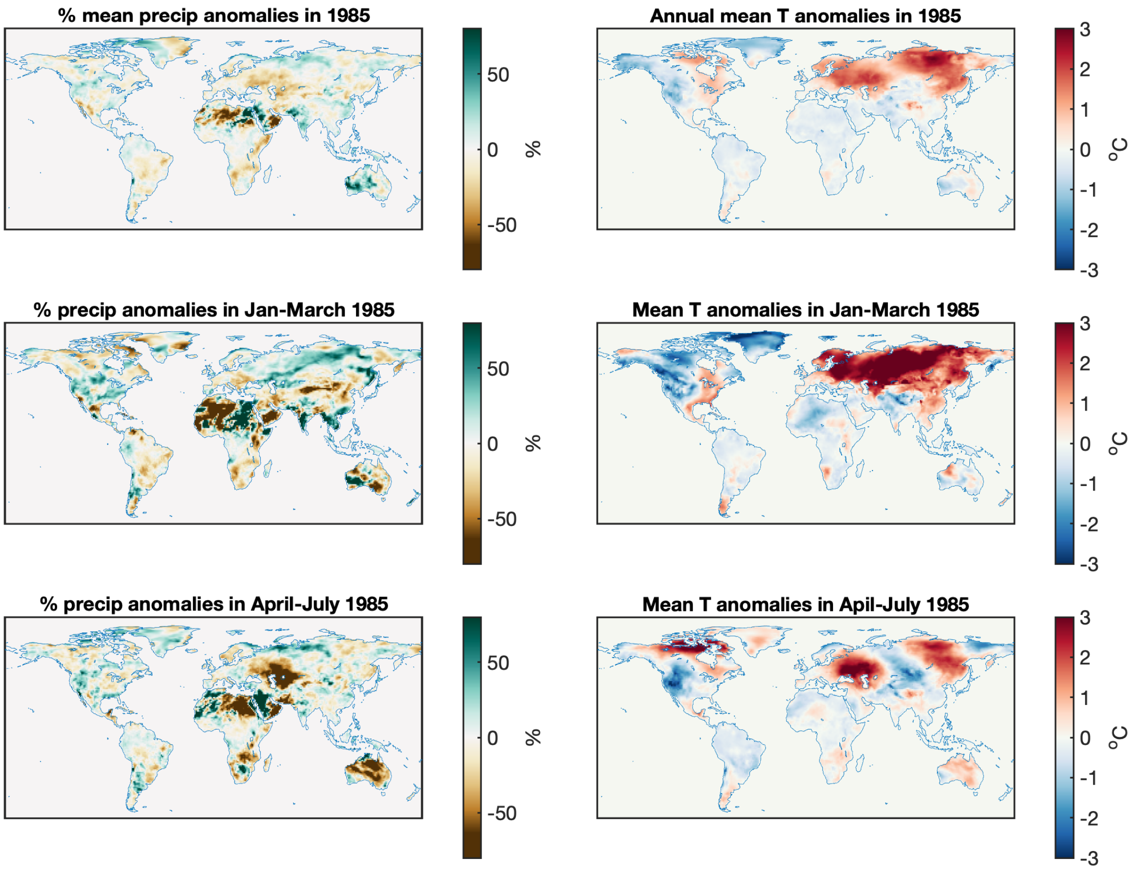

Figure S20 Precipitation and temperature anomalies in 1985. The anomalies were calculated with respect to the mean between 1982 and 1988. Top panels: annual precipitation and temperature anomalies (unit: °C); Middle panel: precipitation and temperature anomalies between January and March 1985; Bottom panel: precipitation and temperature anomalies between April and July 1985.

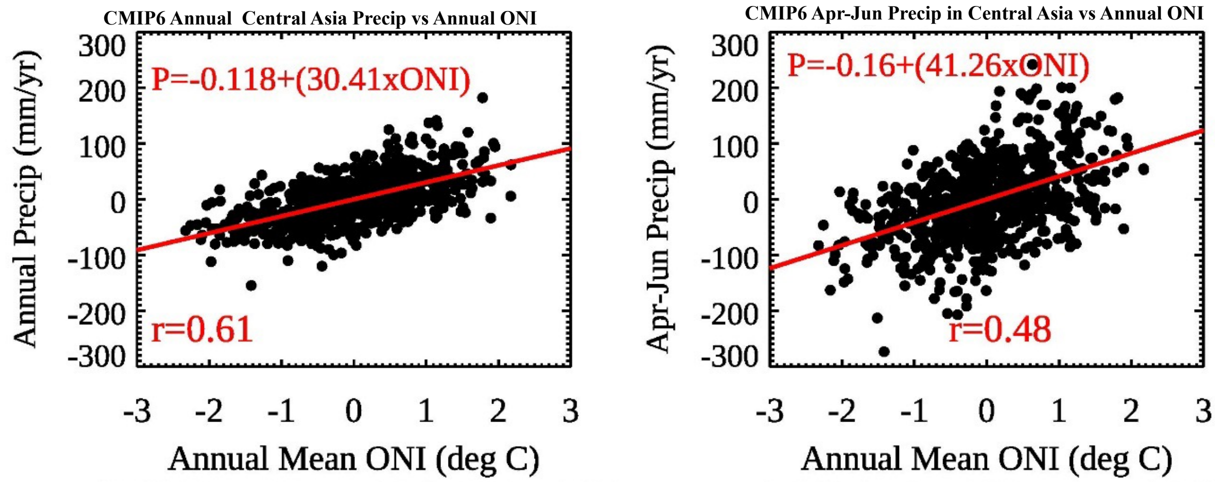

Figure S21 (left) Annual precipitation anomalies over the Central Asian Region (30°E-85°E, 30°N-50°N) versus annual mean Oceanic Niño Index (ONI) for the nine available models from the Coupled Model Intercomparison Project Phase Six (CMIP6) r1i1p1 versions (described further in the text). (Right) Same as the left panel, except April through June precipitation anomalies. Each dot in each plot represents a seasonal or annual precipitation anomaly for each of the individual model years from 2016-2100. To compute the ONI, any possible long-term trend is linearly removed for each model first; analogously this is how precipitation anomalies are computed. The linear correlation coefficients and best-fit lines are shown in each panel. The CMIP6 models used for this analysis are only those which contain r1i1p1 versions, in which "r" refers to the realization (ensemble member), "i" initialization method, and "p" the physics. We utilize nine CMIP6 models (IPSL, CNRM, MPI, NCAR, MRI, CCCMA, MIROC, GFDL, and CAM5). For an overview of the configuration and experimental design of CMIP6, please see (52).

Table S1. Summary of the ensemble of top-down atmospheric inversion models.

Model Name	**Transport Model**	**Resolution**	**Inversion Method**	**Meteorology**	**Prior terrestrial biosphere flux**	**Prior air-sea flux**	**Contact**
NOAA-Baker	PCTM	4° x 5°	4D-Var	MERRA2	CASA-GFED3	Landschutzer v4.4	D. Baker
CAMS	LMDZ	1.9°x3.75°	4D-Var	ERA-5	ORCHIDEE	CMEMS	F. Chevallier
John Hopkins	GEOS-Chem	4° x 5°	Geostastical /4D-Var	MERRA-2	CASA-GFED4.1s	Takahashi	S. Miller
TM5-4Dvar	TM5	2°x3°	4D-Var	ERA-5	SiB-CASA	CT2019	S. Basu
AMES	GEOS-Chem	4° x 5°	4D-Var	MERRA-2	CASA-GFED4.1s	CT2019	S. Philip/M. Johnson
COLA	GEOS-Chem	4°x5°	EnKF	MERRA-2	VEGAS	Rodenbeck2021	N. Zeng/Z. Liu
CMS-Flux	GEOS-Chem	4°x5°	4D-Var	Merra-2	CADAMOM	MOM6	J. Liu
GCASv2	MOZART-4	2.8°x2.8°	EnKF	ERA-5	BEPS	CT2017	F. Jiang

Table S2. List of datasets used in the study.

OCO-2 10sec averages	ftp.cira.colostate.edu:/ftp/BAKER/OCO2_b10c_10sec_GOOD_r7.nc4
Atmospheric CO_2 growth rate	https://gml.noaa.gov/ccgg/trends/gl_gr.html
Fossil fuel emissions	https://zenodo.org/record/8325420
GOSIF	https://globalecology.unh.edu/data/GOSIF.html
FluxSAT	https://daac.ornl.gov/VEGETATION/guides/FluxSat_GPP_FPAR.html#datadescraccess
Nino 3.4 index	https://origin.cpc.ncep.noaa.gov/products/analysis_monitoring/ensostuff/ONI_v5.php
GPCP precipitation	https://www.ncei.noaa.gov/data/global-precipitation-climatology-project-gpcp-monthly/access/
Fire CO2 emissions	https://doi.org/10.6084/m9.figshare.21770624.v1
2-m Temperature and 2-m dew point temperature	ERA-5 reanalysis https://cds.climate.copernicus.eu/cdsapp#!/dataset/reanalysis-era5-land-monthly-means?tab=overview
OCO-2 v10 MIP extension	https://gml.noaa.gov/ccgg/OCO2_v10mip/download.php
ACT-America	https://daac.ornl.gov/cgi-bin/dsviewer.pl?ds_id=1593
CONTRAIL	https://www.nies.go.jp/doi/10.17595/20180208.001-e.html

REFERENCES AND NOTES

1. P. Friedlingstein, M. W. Jones, M. O'Sullivan, R. M. Andrew, D. C. E. Bakker, J. Hauck, C. le Quéré, G. P. Peters, W. Peters, J. Pongratz, S. Sitch, J. G. Canadell, P. Ciais, R. B. Jackson, S. R. Alin, P. Anthoni, N. R. Bates, M. Becker, N. Bellouin, L. Bopp, T. T. T. Chau, F. Chevallier, L. P. Chini, M. Cronin, K. I. Currie, B. Decharme, L. M. Djeutchouang, X. Dou, W. Evans, R. A. Feely, L. Feng, T. Gasser, D. Gilfillan, T. Gkritzalis, G. Grassi, L. Gregor, N. Gruber, Ö. Gürses, I. Harris, R. A. Houghton, G. C. Hurtt, Y. Iida, T. Ilyina, I. T. Luijkx, A. Jain, S. D. Jones, E. Kato, D. Kennedy, K. Klein Goldewijk, J. Knauer, J. I. Korsbakken, A. Körtzinger, P. Landschützer, S. K. Lauvset, N. Lefèvre, S. Lienert, J. Liu, G. Marland, P. C. McGuire, J. R. Melton, D. R. Munro, J. E. M. S. Nabel, S. I. Nakaoka, Y. Niwa, T. Ono, D. Pierrot, B. Poulter, G. Rehder, L. Resplandy, E. Robertson, C. Rödenbeck, T. M. Rosan, J. Schwinger, C. Schwingshackl, R. Séférian, A. J. Sutton, C. Sweeney, T. Tanhua, P. P. Tans, H. Tian, B. Tilbrook, F. Tubiello, G. R. van der Werf, N. Vuichard, C. Wada, R. Wanninkhof, A. J. Watson, D. Willis, A. J. Wiltshire, W. Yuan, C. Yue, X. Yue, S. Zaehle, J. Zeng, Global carbon budget 2021. *Earth Syst. Sci. Data*, **14**, 1917–2005 (2022).

2. N. Zeng, A. Mariotti, P. Wetzel, Terrestrial mechanisms of interannual CO_2 variability. *Global Biogeochem. Cycles* **19**, GB1016 (2005).

3. P. J. Sellers, D. S. Schimel, B. Moore, J. Liu, A. Eldering, Observing carbon cycle–climate feedbacks from space. *Proc. Natl. Acad. Sci. U.S.A.*, **115**, 7860–7868 (2018).

4. J. Worden, S. Saatchi, M. Keller, A. A. Bloom, J. Liu, N. Parazoo, J. B. Fisher, K. Bowman, J. T. Reager, K. Fahy, D. Schimel, R. Fu, S. Worden, Y. Yin, P. Gentine, A. G. Konings, G. R. Quetin, M. Williams, H. Worden, M. Shi, A. Barkhordarian, Satellite observations of the tropical terrestrial carbon balance and interactions with the water cycle during the 21st century. *Rev. Geophys.* **59**, e2020RG000711 (2021).

5. B. Poulter, D. Frank, P. Ciais, R. B. Myneni, N. Andela, J. Bi, G. Broquet, J. G. Canadell, F. Chevallier, Y. Y. Liu, S. W. Running, S. Sitch, G. R. van der Werf, Contribution of semi-arid ecosystems to interannual variability of the global carbon cycle. *Nature* **509**, 600–603 (2014).

6. O. L. Phillips, L. E. O. C. Aragão, S. L. Lewis, J. B. Fisher, J. Lloyd, G. López-González, Y. Malhi, A. Monteagudo, J. Peacock, C. A. Quesada, G. van der Heijden, S. Almeida, I. Amaral, L. Arroyo, G. Aymard, T. R. Baker, O. Bánki, L. Blanc, D. Bonal, P. Brando, J. Chave, A. C OAlves de Oliveira, N. D. Cardozo, C. I. Czimczik, T. R. Feldpausch, M. A. Freitas, E. Gloor, N. Higuchi, E. Jiménez, G. Lloyd, P. Meir, C. Mendoza, A. Morel, D. A. Neill, D. Nepstad, S. Patiño, M. C. Peñuela, A. Prieto, F. Ramírez, M. Schwarz, J. Silva, M. Silveira, A. S. Thomas, H. T. Steege, J. Stropp, R. Vásquez, P. Zelazowski, E. A. Dávila, S. Andelman, A. Andrade, K.-J. Chao, T. Erwin, A. Di Fiore, E. Honorio, H. Keeling, T. J. Killeen, W. F. Laurance, A. P. Cruz, N. C. A. Pitman, P. N. Vargas, H. Ramírez-Angulo, A. Rudas, R. Salamão, N. Silva, J. Terborgh, A. Torres-Lezama, Drought sensitivity of the amazon rainforest. *Science* **323**, 1344–1347 (2009).

7. S. L. Lewis, P. M. Brando, O. L. Phillips, G. M. F. van der Heijden, D. Nepstad, The 2010 amazon drought. *Science* **331**, 554 (2011).

8. J. C. Jiménez-Muñoz, C. Mattar, J. Barichivich, A. Santamaría-Artigas, K. Takahashi, Y. Malhi, J. A. Sobrino, G. van der Schrier, Record-breaking warming and extreme drought in the Amazon rainforest during the course of El Niño 2015–2016. *Sci. Rep.*, **6**, 33130 (2016).

9. K. W. Bowman, J. Liu, A. A. Bloom, N. C. Parazoo, M. Lee, Z. Jiang, D. Menemenlis, M. M. Gierach, G. J. Collatz, K. R. Gurney, D. Wunch, Global and brazilian carbon response to El Niño Modoki 2011–2010. *Earth Sp. Sci.* **4**, 637–660 (2017).

10. J. Wang, N. Zeng, M. Wang, F. Jiang, F. Chevallier, S. Crowell, W. He, M. S. Johnson, J. Liu, Z. Liu, S. M. Miller, S. Philip, H. Wang, M. Wu, W. Ju, S. Feng, M. Jia, Anomalous net biome exchange over amazonian rainforests induced by the 2015/16 El Niño: Soil dryness-shaped spatial pattern but temperature-dominated total flux. *Geophys. Res. Lett.* **50**, e2023GL103379 (2023).

11. J. Liu, K. W. Bowman, D. S. Schimel, N. C. Parazoo, Z. Jiang, M. Lee, A. A. Bloom, D. Wunch, C. Frankenberg, Y. Sun, C. W. O'dell, K. R. Gurney, D. Menemenlis, M. Gierach, D. Crisp, A. Eldering, Contrasting carbon cycle responses of the tropical continents to the 2015–2016 El Niño. *Science* **358**, eaam5690 (2017).

12. B. Byrne, J. Liu, M. Lee, Y. Yin, K. W. Bowman, K. Miyazaki, A. J. Norton, J. Joiner, D. F. Pollard, D. W. T. Griffith, V. A. Velazco, N. M. Deutscher, N. B. Jones, C. Paton-Walsh, The carbon cycle of southeast australia during 2019–2020: Drought, fires, and subsequent recovery. *AGU Adv.*, **2**, e2021AV000469 (2021).

13. H. Peiro, S. Crowell, A. Schuh, D. Baker, C. O'Dell, A. Jacobson, F. Chevallier, J. Liu, A. Eldering, D. Crisp, F. Deng, B. Weir, S. Basu, M. S. Johnson, S. Philip, I. Baker, Four years of global carbon cycle observed from OCO-2 version 9 and in situ data, and comparison to OCO-2 v7. *Atmos. Chem. Phys.*, **2021**, 1–50 (2021).

14. B. Byrne, D. F. Baker, S. Basu, M. Bertolacci, K. W. Bowman, D. Carroll, A. Chatterjee, F. Chevallier, P. Ciais, N. Cressie, D. Crisp, S. Crowell, F. Deng, Z. Deng, N. M. Deutscher, M. K. Dubey, S. Feng, O. E. García, D. W. T. Griffith, B. Herkommer, L. Hu, A. R. Jacobson, R. Janardanan, S. Jeong, M. S. Johnson, D. B. A. Jones, R. Kivi, J. Liu, Z. Liu, S. Maksyutov, J. B. Miller, S. M. Miller, I. Morino, J. Notholt, T. Oda, C. W. O'Dell, Y. S. Oh, H. Ohyama, P. K. Patra, H. Peiro, C. Petri, S. Philip, D. F. Pollard, B. Poulter, M. Remaud, A. Schuh, M. K. Sha, K. Shiomi, K. Strong, C. Sweeney, Y. Té, H. Tian, V. A. Velazco, M. Vrekoussis, T. Warneke, J. R. Worden, D. Wunch, Y. Yao, J. Yun, A. Zammit-Mangion, N. Zeng, National CO2 budgets (2015--2020) inferred from atmospheric CO2 observations in support of the global stocktake. *Earth Syst. Sci. Data*, **15**, 963–1004 (2023).

15. F. Jiang, H. Wang, J. M. Chen, W. Ju, X. Tian, S. Feng, G. Li, Z. Chen, S. Zhang, X. Lu, J. Liu, H. Wang, J. Wang, W. He, M. Wu, Regional CO_2 fluxes from 2010 to 2015 inferred from GOSAT XCO_2 retrievals using a new version of the global carbon assimilation system. *Atmos. Chem. Phys.*, **21**, 1963–1985 (2021).

16. W. He, F. Jiang, W. Ju, B. Byrne, J. Xiao, N. T. Nguyen, M. Wu, S. Wang, J. Wang, C. Rödenbeck, X. Li, M. Scholze, G. Monteil, H. Wang, Y. Zhou, Q. He, J. M. Chen, Do State-Of-The-Art Atmospheric CO_2 Inverse Models Capture Drought Impacts on the European Land Carbon Uptake? *J. Adv. Model. Earth Syst.*, **15**, e2022MS003150 (2023).

17. P. Friedlingstein, M. O'Sullivan, M. W. Jones, R. M. Andrew, L. Gregor, J. Hauck, C. le Quéré, I. T. Luijkx, A. Olsen, G. P. Peters, W. Peters, J. Pongratz, C. Schwingshackl, S. Sitch, J. G.

Canadell, P. Ciais, R. B. Jackson, S. R. Alin, R. Alkama, A. Arneth, V. K. Arora, N. R. Bates, M. Becker, N. Bellouin, H. C. Bittig, L. Bopp, F. Chevallier, L. P. Chini, M. Cronin, W. Evans, S. Falk, R. A. Feely, T. Gasser, M. Gehlen, T. Gkritzalis, L. Gloege, G. Grassi, N. Gruber, Ö. Gürses, I. Harris, M. Hefner, R. A. Houghton, G. C. Hurtt, Y. Iida, T. Ilyina, A. K. Jain, A. Jersild, K. Kadono, E. Kato, D. Kennedy, K. Klein Goldewijk, J. Knauer, J. I. Korsbakken, P. Landschützer, N. Lefèvre, K. Lindsay, J. Liu, Z. Liu, G. Marland, N. Mayot, M. J. McGrath, N. Metzl, N. M. Monacci, D. R. Munro, S. I. Nakaoka, Y. Niwa, K. O'Brien, T. Ono, P. I. Palmer, N. Pan, D. Pierrot, K. Pocock, B. Poulter, L. Resplandy, E. Robertson, C. Rödenbeck, C. Rodriguez, T. M. Rosan, J. Schwinger, R. Séférian, J. D. Shutler, I. Skjelvan, T. Steinhoff, Q. Sun, A. J. Sutton, C. Sweeney, S. Takao, T. Tanhua, P. P. Tans, X. Tian, H. Tian, B. Tilbrook, H. Tsujino, F. Tubiello, G. R. van der Werf, A. P. Walker, R. Wanninkhof, C. Whitehead, A. Willstrand Wranne, R. Wright, W. Yuan, C. Yue, X. Yue, S. Zaehle, J. Zeng, B. Zheng, Global Carbon Budget 2022. *Earth Syst. Sci. Data*, **14**, 4811–4900 (2022).

18. C. Rödenbeck, S. Houweling, M. Gloor, M. Heimann, CO_2 flux history 1982–2001 inferred from atmospheric data using a global inversion of atmospheric transport. *Atmos. Chem. Phys.*, **3**, 1919–1964 (2003).

19. P. Bousquet, P. Peylin, P. Ciais, C Le Quéré, P. Friedlingstein, P P Tans, Regional Changes in Carbon Dioxide Fluxes of Land and Oceans Since 1980. *Science* **290**, 1342–1347 (2000).

20. D. F. Baker, R. M. Law, K. R. Gurney, P. Rayner, P. Peylin, A. S. Denning, P. Bousquet, L. Bruhwiler, Y. H. Chen, P. Ciais, I. Y. Fung, M. Heimann, J. John, T. Maki, S. Maksyutov, K. Masarie, M. Prather, B. Pak, S. Taguchi, Z. Zhu, TransCom 3 inversion intercomparison: Impact of transport model errors on the interannual variability of regional CO2 fluxes, 1988–2003. *Global Biogeochem. Cycles*, **20** https://doi.org/https://doi.org/10.1029/2004GB002439 (2006).

21. R. J. Leamon, The triple-dip La Niña of 2020–22: Updates to the correlation of ENSO with the termination of solar cycles. *Front. Earth Sci.*, **11** https://doi.org/10.3389/feart.2023.1204191 (2023).

22. C. Gao, M. Chen, L. Zhou, L. Feng, R. H. Zhang, The 2020–2021 prolonged La Niña evolution in the tropical Pacific. *Sci. China Earth Sci.*, **65**, 2248–2266 (2022).

23. B. Gaubert, B. B. Stephens, S. Basu, F. Chevallier, F. Deng, E. A. Kort, P. K. Patra, W. Peters, C. Rödenbeck, T. Saeki, D. Schimel, I. Van der Laan-Luijkx, S. Wofsy, Y. Yin,, Global atmospheric CO_2 inverse models converging on neutral tropical land exchange but diverging on fossil fuel and atmospheric growth rate. *Biogeosciences* **16** 117–134 (2018).

24. B. B. Stephens, K. R. Gurney, P. P. Tans, C. Sweeney, W. Peters, L. Bruhwiler, P. Ciais, M. Ramonet, P. Bousquet, T. Nakazawa, S. Aoki, T. Machida, G. Inoue, N. Vinnichenko, J. Lloyd, A. Jordan, M. Heimann, O. Shibistova, R. L. Langenfelds, L Paul Steele, R. J. Francey, A. S. Denning, Weak northern and strong tropical land carbon uptake from vertical profiles of atmospheric CO_2. *Science* **316**, 1732–1735 (2007).

25. A. E. Schuh, A. R. Jacobson, Uncertainty in parameterized convection remains a key obstacle for estimating surface fluxes of carbon dioxide. *Atmos. Chem. Phys.*, **23**, 6285–6297 (2023).

26. B. Zheng, P. Ciais, F. Chevallier, H. Yang, J. G. Canadell, Y. Chen, I. R. van der Velde, I. Aben, E. Chuvieco, S. J. Davis, M. Deeter, C. Hong, Y. Kong, H. Li, H. Li, X. Lin, K. He, Q. Zhang, Record-high CO_2 emissions from boreal fires in 2021. *Science* **379**, 912–917 (2023).

27. A. A. Bloom, J.-F. Exbrayat, I. R. van der Velde, L. Feng, M. Williams, The decadal state of the terrestrial carbon cycle: Global retrievals of terrestrial carbon allocation, pools, and residence times. **113**, 1285–1290 (2016).

28. N. Madani, J. S. Kimball, N. C. Parazoo, A. P. Ballantyne, T. Tagesson, L. A. Jones, R. H. Reichle, P. I. Palmer, I. Velicogna, A. A. Bloom, S. Saatchi, Z. Liu, A. Geruo, Below-surface water mediates the response of African forests to reduced rainfall. *Environ. Res. Lett.*, **15**, 34063 (2020).

29. B. D. Stocker, S. J. Tumber-Dávila, A. G. Konings, M. C. Anderson, C. Hain, R. B. Jackson, Global patterns of water storage in the rooting zones of vegetation. *Nat. Geosci.*, **16**, 250–256 (2023).

30. Y. Fan, G. Miguez-Macho, E. G. Jobbágy, R. B. Jackson, C. Otero-Casal, Hydrologic regulation of plant rooting depth. *Proc. Natl. Acad. Sci. U.S.A.*, **114**, 10572 (2017).

31. T. Zhou, W. Zhang, L. Zhang, R. Clark, C. Qian, Q. Zhang, H. Qiu, J. Jiang, X. Zhang, 2021: A year of unprecedented climate extremes in Eastern Asia, North America, and Europe. *Adv. Atmos. Sci.*, **39**, 1598–1607 (2022).

32. A. Bastos, I. A. Janssens, C. M. Gouveia, R. M. Trigo, P. Ciais, F. Chevallier, J. Peñuelas, C. Rödenbeck, S. Piao, P. Friedlingstein, S. W. Running, European land CO_2 sink influenced by NAO and East-Atlantic Pattern coupling. *Nat. Commun.*, **7**, 10315 (2016).

33. J. Wang, M. Wang, J. S. Kim, J. Joiner, N. Zeng, F. Jiang, H. Wang, W. He, M. Wu, T. Chen, W. Ju, J. M. Chen, Modulation of land photosynthesis by the indian ocean dipole: Satellite-based observations and CMIP6 future projections. *Earth's Futur.*, **9**, e2020EF001942 (2021).

34. J.-S. Kim, J.-S. Kug, S.-J. Jeong, H. Park, G. Schaepman-Strub, Extensive fires in southeastern Siberian permafrost linked to preceding Arctic Oscillation. *Sci. Adv.*, **6**, eaax3308 (2020).

35. R. J. Andres, T. A. Boden, D. M. Higdon, Gridded uncertainty in fossil fuel carbon dioxide emission maps, a CDIAC example. *Atmos. Chem. Phys.*, **16**, 14979–14995 (2016).

36. A. P. Ballantyne, R. Andres, R. Houghton, B. D. Stocker, R. Wanninkhof, W. Anderegg, L. A. Cooper, M. DeGrandpre, P. P. Tans, J. B. Miller, C. Alden, J. W. C. White, Audit of the global carbon budget: Estimate errors and their impact on uptake uncertainty. *Biogeosciences*, **12**, 2565–2584 (2015).

37. M. G. Bosilovich, F. R. Robertson, P. W. Stackhouse, El Niño–Related Tropical Land Surface Water and Energy Response in MERRA-2. *J. Climate*, **33**, 1155–1176 (2020).

38. P. M. Cox, D. Pearson, B. B. Booth, P. Friedlingstein, C. Huntingford, C. D. Jones, C. M. Luke, Sensitivity of tropical carbon to climate change constrained by carbon dioxide variability. *Nature*, **494**, 341–344 (2013).

39. A. Barkhordarian, K. W. Bowman, N. Cressie, J. Jewell, J. Liu, Emergent constraints on tropical atmospheric aridity–carbon feedbacks and the future of carbon sequestration. *Environ. Res. Lett.* **16** 114008 (2021).

40. W. Cai, G. Wang, A. Santoso, M. J. McPhaden, L. Wu, F. F. Jin, A. Timmermann, M. Collins, G. Vecchi, M. Lengaigne, M. H. England, D. Dommenget, K. Takahashi, E. Guilyardi, Increased frequency of extreme La Niña events under greenhouse warming. *Nat. Clim. Chang.*, **5**, 132–137 (2015).

41. S. Basu, R. Nassar, *Fossil Fuel* CO_2 *Emissions for the OCO2 Model Intercomparison Project (MIP)*. 10.5281/zenodo.8325420 (2023).

42. C. L. Quéré, R. M. Andrew, P. Friedlingstein, S. Sitch, J. Pongratz, A. C. Manning, J. I. Korsbakken, G. P. Peters, J. G. Canadell, R. B. Jackson, T. A. Boden, P. P. Tans, O. D. Andrews, V. K. Arora, D. C. E. Bakker, L. Barbero, M. Becker, R. A. Betts, L. Bopp, F. Chevallier, L. P. Chini, P. Ciais, C. E. Cosca, J. Cross, K. Currie, T. Gasser, I. Harris, J. Hauck, V. Haverd, R. A. Houghton, C. W. Hunt, G. Hurtt, T. Ilyina, A. K. Jain, E. Kato, M. Kautz, R. F. Keeling, K. K. Goldewijk, A. Körtzinger, P. Landschützer, N. Lefèvre, A. Lenton, S. Lienert, I. Lima, D. Lombardozzi, N. Metzl, F. Millero, P. M. S. Monteiro, D. R. Munro, J. E. M. S. Nabel, S.-I. Nakaoka, Y. Nojiri, X. A. Padin, A. Peregon, B. Pfeil, D. Pierrot, B. Poulter, G. Rehder, J. Reimer, C. Rödenbeck, J. Schwinger, R. Séférian, I. Skjelvan, B. D. Stocker, H. Tian, B. Tilbrook, F. N. Tubiello, I. T. van der Laan-Luijkx, G. R. van der Werf, S. van Heuven, N. Viovy, N. Vuichard, A. P. Walker, A. J. Watson, A. J. Wiltshire, S. Zaehle, D. Zhu, Global Carbon Budget 2017. *Earth Syst. Sci. Data*, **10**, 405–448 (2018).

43. K. J. Davis, M. D. Obland, B. Lin, T. Lauvaux, C. O'Dell, B. Meadows, E. V. Browell, J. P. DiGangi, C. Sweeney, M. J. McGill, J. D. Barrick, A. R. Nehrir, M. M. Yang, J. R. Bennett, B. C. Baier, A. Roiger, S. Pal, T. Gerken, A. Fried, S. Feng, R. Shrestha, M. A. Shook, G. Chen, L. J. Campbell, Z. R. Barkley, R. M. Pauly, *ACT-America: L3 Merged In Situ Atmospheric Trace Gases and Flask Data, Eastern USA*. 10.3334/ORNLDAAC/1593 (2018).

44. Y. Wei, R. Shrestha, S. Pal, T. Gerken, S. Feng, J. McNelis, D. Singh, M. M. Thornton, A. G. Boyer, M. A. Shook, G. Chen, B. C. Baier, Z. R. Barkley, J. D. Barrick, J. R. Bennett, E. V. Browell, J. F. Campbell, L. J. Campbell, Y. Choi, J. Collins, J. Dobler, M. Eckl, A. Fiehn, A. Fried, J. P. Digangi, R. Barton-Grimley, H. Halliday, T. Klausner, S. Kooi, J. Kostinek, T. Lauvaux, B. Lin, M. J. McGill, B. Meadows, N. L. Miles, A. R. Nehrir, J. B. Nowak, M. Obland,

C. O'Dell, R. M. P. Fao, S. J. Richardson, D. Richter, A. Roiger, C. Sweeney, J. Walega, P. Weibring, C. A. Williams, M. M. Yang, Y. Zhou, K. J. Davis, Atmospheric Carbon and Transport–America (ACT-America) Data Sets: Description, Management, and Delivery. *Earth Space Sci.*, **8**, e2020EA001634 (2021).

45. K. J. Davis, E. V. Browell, S. Feng, T. Lauvaux, M. D. Obland, S. Pal, B. C. Baier, D. F. Baker, I. T. Baker, Z. R. Barkley, K. W. Bowman, Y. Y. Cui, A. S. Denning, J. P. DiGangi, J. T. Dobler, A. Fried, T. Gerken, K. Keller, B. Lin, A. R. Nehrir, C. P. Normile, C. W. O'Dell, L. E. Ott, A. Roiger, A. E. Schuh, C. Sweeney, Y. Wei, B. Weir, M. Xue, C. A. Williams, The Atmospheric Carbon and Transport (ACT)-America Mission. *Bull. Am. Meteorol. Soc.*, **102**, E1714–E1734 (2021).

46. B. C. Baier, C. Sweeney, Y. Choi, K. J. Davis, J. P. DiGangi, S. Feng, A. Fried, H. Halliday, J. Higgs, T. Lauvaux, B. R. Miller, S. A. Montzka, T. Newberger, J. B. Nowak, P. Patra, D. Richter, J. Walega, P. Weibring, Multispecies assessment of factors influencing regional CO_2 and CH_4 enhancements during the winter 2017 ACT-America campaign. *J. Geophys. Res. Atmos.*, **125**, e2019JD031339 (2020).

47. T. Machida, H. Matsueda, Y. Sawa, Y. Nakagawa, K. Hirotani, N. Kondo, K. Goto, T. Nakazawa, K. Ishikawa, T. Ogawa, Worldwide measurements of atmospheric CO_2 and other trace gas species using commercial airlines. *J. Atmos. Oceanic Tech.*, **25**, 1744–1754 (2008).

48. J. Joiner, Y. Yoshida, Agricultural and Forest Meteorology Satellite-based re fl ectances capture large fraction of variability in global gross primary production (GPP) at weekly time scales. *Agric. For. Meteorol.* **291**, 108092 (2020).

49. X. Li, J. Xiao, Mapping photosynthesis solely from solar-induced chlorophyll fluorescence: A global, fine-resolution dataset of gross primary production derived from OCO-2. *Remote Sens. (Basel)* **11**, 2563 (2019).

50. B. Zheng, *Global fire CO2 emissions 2000–2021*. 10.6084/m9.figshare.21770624.v1 (2022).

51. L. Gu, D. D. Baldocchi, S. C. Wofsy, J William Munger, J. J. Michalsky, S. P. Urbanski, T. A. Boden, Response of a deciduous forest to the mount pinatubo eruption: Enhanced photosynthesis. *Science* **299**, 2035–2038 (2003).

52. V. Eyring, S. Bony, G. A. Meehl, C. A. Senior, B. Stevens, R. J. Stouffer, K. E. Taylor, Overview of the coupled model intercomparison project phase 6 (CMIP6) experimental design and organization. *Geosci. Model Dev.*, **9**, 1937–1958 (2016).